RESEARCH ARTICLE

Check for updates

Development and characterization of functionalized glyco thiolate capped gold nanoparticles for biological applications†

Christian K. Adokoh, [iD] ‡*[a] Frankline K. Keter,§[b] Henok H. Kinfe [iD] [a] Robert Tshikhudo[b] and James Darkwa*[a]

Glyco-gold nanoparticles (AuNPs) in aqueous dispersions were prepared by two approaches, namely direct reduction and ligand substitution methods. In the direct method, potassium salts of glyco thiols, with the general formula $(C_6H_{11}O_6)NH(CH_2)_nCH_2SK$ (where L1, $n = 1$; L2, $n = 2$; L3, $n = 3$, L4, $n = 4$; L5, $n = 5$), were used as reducing and capping agents to give the glyco thiolate capped gold nanoparticles (AuNPs G1–G5); meanwhile in the ligand exchange experiments, L1–L5 and their acetylated forms (L6–L8) replaced citrate ions in citrate-capped gold nanoparticles to give additional AuNPs G6–G11. UV-visible spectroscopy, surface charge (ζ-potential,) measurements and transmission electron microscopy (TEM) were used for physical and chemical characterization of all the resultant AuNPs. The ζ-potential studies of AuNPs prepared through the direct method revealed that the surface charge is dependent on the length of the alkyl unit of $(C_6H_{11}O_6)NH(CH_2)_nCH_2S^-$ ligands. TEM images of the acetylated and non-acetylated glyco thiolate capped gold nanoparticles (AuNPs G6–G11) prepared via the ligand exchange method indicate that the size and shape of the gold nanoparticles remained the same as those of the citrate-capped gold nanoparticles used to prepare them. Selected AuNPs were tested on peripheral blood mononuclear cells (PBMCs) and the A549 cancer cell line to investigate their respective toxicity and cytotoxicity profiles. All AuNPs showed indiscriminate activity against both PBMCs and A4549 cells, although the gold nanoparticles having an acetylated glyco moiety with an amino propyl thiol linker as the ligand (G10) prepared via the citrate exchange method had better selectivity (PBMCs >59 mg mL^{-1} and for A549 ~7 μg mL^{-1}).

Introduction

The unique properties and wide range of potential applications of metal-based nanomaterials are of huge interest to the scientific community. In particular, gold nanoparticles have aroused attention due to their applications in optoelectronics,[1] drug delivery,[2] chemical sensing,[3] catalysis,[4] nano electronics[5] and medical diagnostics.[6] However, the synthesis of small, monodisperse nanoparticles is a major challenge, considering the fact that small particles experience increased driving force to aggregate.[7] As such, engineering the surface of the nanoparticles to achieve monodispersity is of paramount importance. To achieve this, protective coating or "capping" is necessary during synthesis to keep the nanoparticles in a finely dispersed state. The most common method for the synthesis of monodispersed spherical gold nanoparticles was demonstrated by Turkevich et al. (1951)[7] and later refined by Frens et al. (1972 and 1973)[8,9] where gold salts, such as HAuCl$_4$, were chemically reduced using various sodium salts. This method produces monodispersed spherical gold nanoparticles with a diameter of ~10–20 nm, depending on the anion in the sodium salt. For example, trisodium citrate produces gold nanoparticles that have a diameter of ~14 nm. These gold nanoparticles can be further modified with other surfactants/ stabilizers, e.g. polyethylene glycol (PEG), to improve their stability. Furthermore, other gold nanoparticles of different shapes (i.e. triangular, polygonal rods and spherical particles) have also been reported.[10–13] These gold nanomaterials have unique properties characterized by their high surface area to volume ratios and have a wide range of applications.[10–14]

Recently, the use of carbohydrates as stabilizing agents for gold nanoparticles has drawn interest not only due to their PEG-like biocompatibility, but also their involvement in cell-mediated interactions.[15–18] In view of this, many thiol-modified

[a] Department of Chemistry, University of Johannesburg, P. O. Box 524, Auckland Park, 2006, South Africa. E-mail: cadokoh@ucc.edu.gh, jdarkwa@gmail.com

[b] Nanotechnology Innovation Center, Advanced Materials Division, Mintek, 200 Malibongwe Drive, Randburg, 2125, South Africa

† Electronic supplementary information (ESI) available. See DOI: 10.1039/ c9md00493a

‡ Current Address: Department of Forensic Sciences, School of Biological Sciences, College of Agriculture and Natural Sciences, University of Cape Coast, Cape Coast, Ghana.

§ Current Address: Africa Resource Centre, 17 Dock Road, V & A Waterfront, Cape Town, 8001, South Africa.
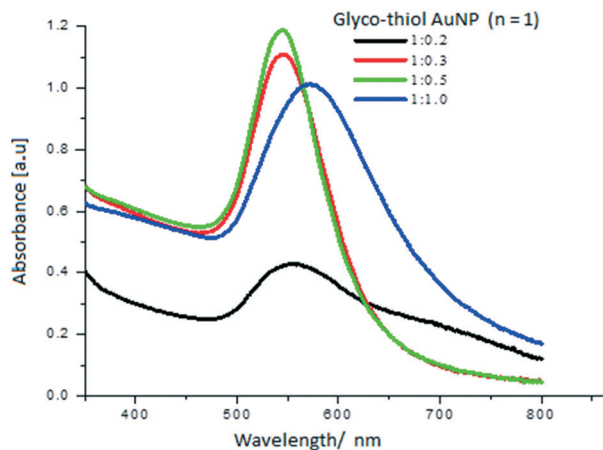
Fig. 1 UV-vis spectra of AuNPs produced with different Au : **L1** ratios.

oligonucleotides have been employed to functionalize gold nanoparticles for detection of nucleic acid sequences in biological samples.[19] Furthermore, carbohydrate-labeled polymers, nanoparticles, galactosylated liposomes and poly(amino acids) have been investigated for their drug delivery capabilities to specific cells and tissues.[20,21] For instance, glyco-based nano-sized materials are now used to target endogenous lectins, which are carbohydrate-binding proteins.[20–23]

In this regard, we recently reported the synthesis and cyto-toxicity study of novel AuNPs stabilized by non-toxic thio-carbohydrates *via* NaBH$_4$ reduction of Au^{3+} to Au^{1+}.[24] In continuation of our efforts in the synthesis of bioactive nanoparticles, we herein report alternative milder methodologies for the synthesis of AuNPs *via* ligand exchange and using thiocarbohydrates as reducing and stabilizing agents without the need for NaBH$_4$, as well as the results of the detailed characterization of the nanoparticles so-synthesised and their cytotoxicity investigation.

Results and discussion

Synthesis of gold nanoparticles using glyco thiolates as reducing and capping agents

Gold nanoparticles (**G1–G3**) were prepared *via* the direct chemical reduction method reported by Turkevich *et al.*

(1951),[7] but using glycothiolate ligands in this study. The gluconamidoalkyl thiol ligands (**L1–L5**) were used to reduce Au(III) ions and as capping agents, too. The reduction of Au(III) may be possible *via* formation of intermediate gold(I) thiolate. All the reactions were performed at 100 °C. At the onset, the reactions were found to be somewhat slow and led to aggregation, as hinted by the observed precipitation at the 8 h mark. The UV-vis data obtained for **G1–G3** showed a broad surface plasmon resonance peak (spr) at 557 nm, which is indicative of aggregation (*cf.* Fig. 1, black trace). The slow nature of the reactions is attributed to the less reactive form of the thiol ligand (with protonated sulfur). Even though thiolates may allow the synthesis to occur in fewer steps, as a result of *in situ* deprotonation during the reaction, there was a need to prepare more reactive analogues of the glycol ligands. Consequently, potassium salts of **L1–L5** were prepared by reacting stoichiometric equimolar amounts of KOH and the ligands, and used *in situ* (Scheme 1). Potassium salts of **L1** and **L2** reduced tetrachloroauric acid. Thus, KOH not only led to the formation of potassium salts of **L1** and **L2**, but also provided a basic condition that further improved the rate of the reaction. Thus, at higher pH (high basicity) re-inforcement of static stabilization is predicted.[25] The colour of the resultant AuNPs ranged from reddish purple to red-dish orange depending on the particle size. The UV-vis data show the spr bands between 532 nm and 609 nm for the AuNPs (**G1** and **G2**), respectively (Fig. 1, Table 1), suggesting that the particles are relatively large.

In order to prepare the AuNPs (**G1** and **G2**) of various sizes, different gold : ligand ratios were used as listed in Table 1. It is interesting to note that contrary to the expecta-tions that an increase in the concentration of the reducing agent would lead to smaller particles, it was not the case with **L1** and **L2** as the formation of nanoparticles was only achieved when the Au^{3+} amount was higher than **L1** or **L2**. It is possible that the increase in ligand concentration favours hydrogen bonding through the hydroxyl groups, thereby expe-diting the aggregation of the particles. In addition, the short length of the alkyl chain of ligands **L1** ($n = 1$) and **L2** ($n = 2$) may allow close interaction of the AuNPs, thereby accelerat-ing the aggregation. This, presumably, is the reason why the formation of **G1** and **G2** AuNPs was observed at very low

Compds.	L1	L2	L3	L4	L5
n	1	2	3	4	5
AuNPs	G1	G2	G3	G4	G5
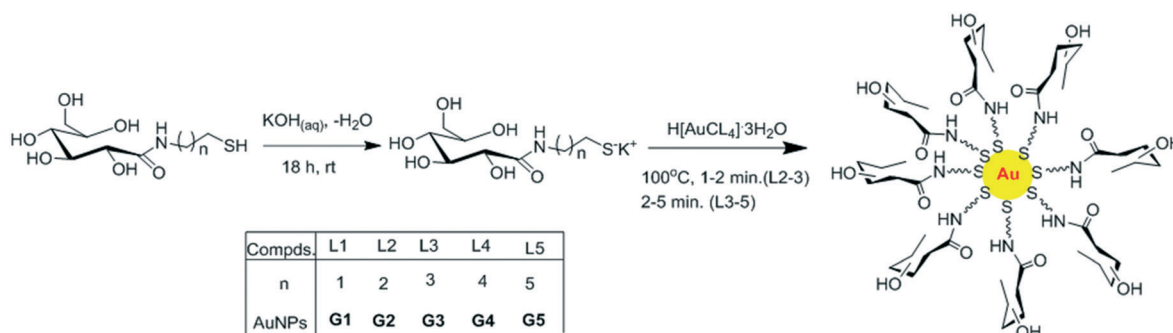
Scheme 1   General representation of gold nanoparticle synthesis.

Table 1 Summary of size (nm), ζ-potential (mV) and λ_{max} for **G1** and **G2**

Parameters	**G1** ($n = 1$)				**G2** ($n = 2$)			
Au:L	1:0.2	1:0.3	1:0.5	1:1	1:0.5	1:0.6	1:0.8	1:1
L mass (mg)	1.1	1.8	3.5	7.0	3.4	4.1	5.5	6.8
Size/nm	37.9 ± 4.5	44.6 ± 16.8	48.9 ± 8.9	—	14.1 ± 2.9	55.4 ± 2.6	AG	AG
ζ/mV	−25.1	−33.3	−27.2	−32.3	−27.9	−27.9	−31.4	−29.7
$\lambda_{max.}$/nm	551	545	545	559	558	551	532	536

concentrations of the ligands (Table 1), albeit with poor dispersion and irregular shapes (Fig. 2).

To investigate whether the length of the alkyl moiety in **G1** and **G2** favoured aggregation as postulated above, the potassium salt of **L3** with a longer alkyl chain ($n = 3$) was used. The particle formation was concentration-dependent such that at high concentrations of **L3** salt, smaller sizes of AuNPs were formed and *vice versa* (Table 2) as expected. This observation was supported by UV-vis data (Fig. 3) where the spr band exhibited a blue shift with an increase in **L3** concentration. Furthermore, TEM data (Fig. 4) not only showed that the particles are of different sizes, between 20.0 and 25.0 nm depending on the gold:ligand ratio (Table 2), but also predominantly spherical and monodisperse. The TEM images show conclusively that **G3** particles are monodispersed (Fig. 4). It is also important to note that the ζ-potential measurements of these AuNPs, which are largely positive, further confirm the monodispersed nature of the nanoparticles (Table 2). It is also noteworthy that the nanoparticle formation was not only concentration dependent but also time dependent. For instance, the reaction with a gold:ligand ratio of 1:3 required approximately 2 h to achieve completion, while those of 1:4, 1:5 and 1:6 required 2.5, 4.5 and 5 h, respectively. This is likely due to the fact that the high concentration of glyco thiols hinders the Ostwald ripening process of nanoparticles because of the diffusion of molecules in between formation.[26]

To further validate the effect of the long chain on nanoparticle formation, **L4** ($n = 4$) and **L5** ($n = 5$) were also used to produce **G4** and **G5**, which showed better defined and smaller particles at high concentrations of **L4** and **L5** (Table 2 and Fig. S1 and S2†), once again emphasizing that the length of the glyco-aliphatic chain plays a critical role in nanoparticle stabilization.

One fundamental characteristic of the nanoparticles formed by glyco aliphatic chains ($n = 3$–5) is their cationic nature compared to shorter chains which were anionic. This is strongly attributed to the influence of the +I effect of the −CH$_2$ chains compared to shorter chains (*i.e.* electron-releasing character of the longer alkyl chains).[27] In addition, a high concentration of the base is also required to form the salt, making the solution more basic (Table 3).

Synthesis of glyco thiolated gold nanoparticles (G6–G11) *via* ligand exchange

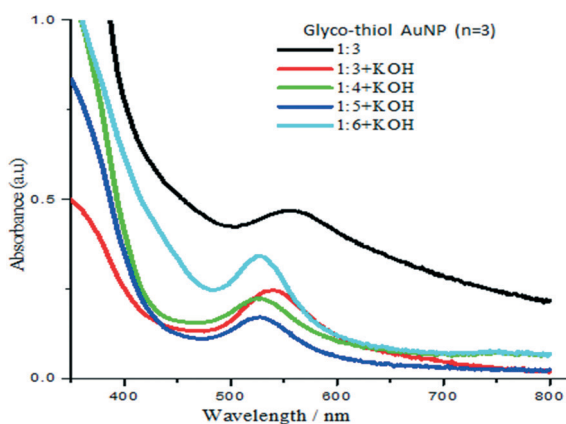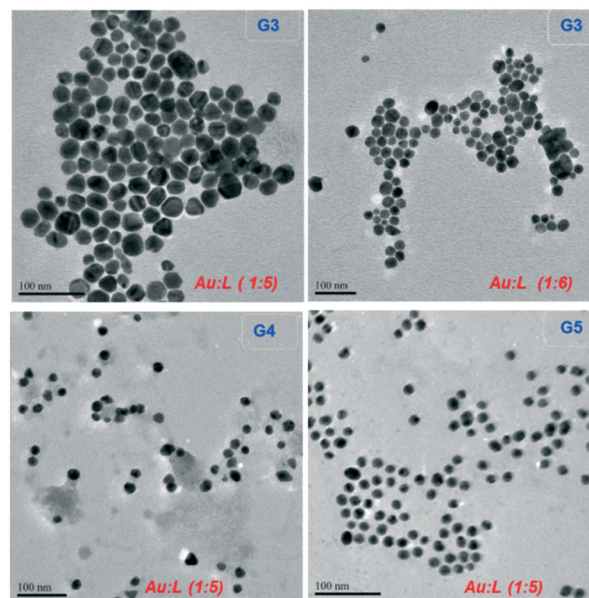14 nm citrate-capped AuNPs were prepared using literature procedures.[7] The particles were analyzed by UV-vis and TEM
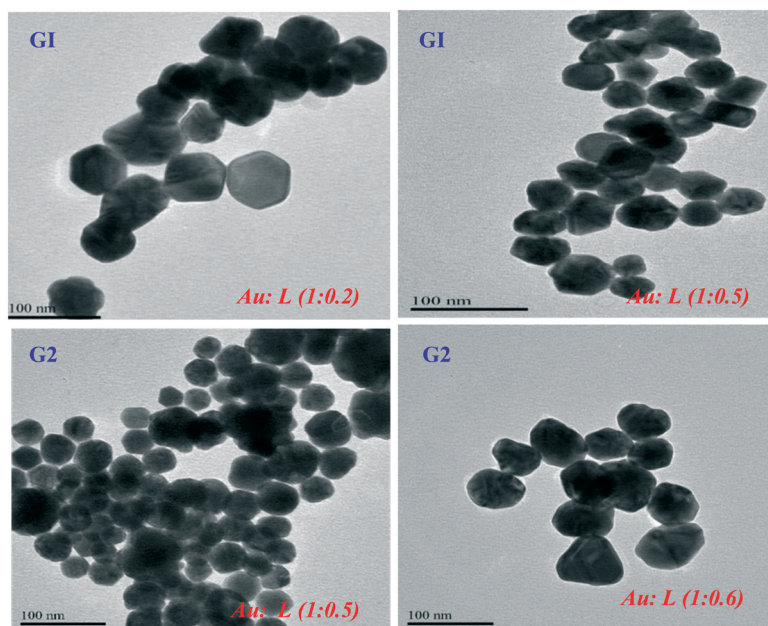
Fig. 2 TEM images of AuNPs of (**G1**) Au:glyco thiol ligand (**L1**) ratios of 1:0.2 and 1:0.5. (**G2**) Au:**L2** of 1:0.5 and 1:0.6, respectively.

Table 2 Summary of size (nm), ζ potential (mV) and λ_{max} for **G3–G5** synthesized from potassium salts of glyco-thiols

Parameters	**G3** ($n = 3$)				**G4** ($n = 4$)		**G5** ($n = 5$)	
Au : L	1 : 3	1 : 4	1 : 5	1 : 6	1 : 3	1 : 5	1 : 3	1 : 5
L mass (mg)	21.0	28.1	35.1	42.1	22.0	36.9	23.2	38.6
Size/nm	25 ± 4	23 ± 3	22 ± 4	20 ± 3	19 ± 3	16 ± 4	16 ± 5	15 ± 4
ξ-Potential/mV	47.0	28.3	40.1	49.5	32.9	35.7	43.1	44.5
λ_{max}/nm	529	527	527	524	538	529	534	531

and found to be monodisperse with an average size of 14 ± 2 nm (Table 3, Fig. S3†). The resultant 14 nm AuNPs were subsequently reacted with **L1–L3** at room temperature as described in the experimental section (Scheme 2). The TEM-EDX data further showed the presence of sulphur, confirming the successful replacement of citrate with the glyco-ligands. The excess unreacted ligands were removed by centrifuging the samples, discarding the supernatant, and the particles were re-suspended in d-H$_2$O.

Attempts to replace citrate surfactants on the AuNPs with un-acetylated **L1–L3** were unsuccessful as the AuNPs aggregated. Just as in the case of **G1–G3**, this is attributed to hydrogen bonding promoted by the hydroxyl groups in the carbohydrate moiety leading to close contact of the AuNPs, thus resulting in aggregation. This necessitated the assessment of the hydrogen bonding effect of **L1–L3** ligands on the nanoparticle formation. This was studied indirectly by pH adjustment experiments where the pH values of ligands **L1–L3** were adjusted incrementally from 7 to 11 using 2 M KOH (*ca.* Table 3). At a high pH of *ca.* 11, stable AuNPs (**G6–G8**) were isolated (*ca.* TEM images in Fig. S3†); this is because, at high pH, the negative charge inferred on the ligands sustains some electrostatic repulsion between ligands and *vice versa*.[28–30] There were marginal shifts of the absorption bands of AuNPs **G6–G8** (521–535 nm) (Fig. 5) compared to the citrate-capped gold nanoparticles (519 nm) which shows that the ligand substitution process did not have much effect on the integrity of the AuNPs (Table 3). The marginal shift in the spr band is purely attributed to the change of the ligand on the surface of the nanoparticles.

**Fig. 4** TEM image of AuNPs (**G3–G5**) from potassium salts of **L3–L5**.

The hydrogen bond effect was further probed using an acetylated form of **L1–L3**, *i.e.* **L6–L8**. Ligands **L6–L8** formed stable AuNPs **G9–G11**. The improved ζ-potential values (−24.5, −26.4 and −30.4 mV) for these AuNPs were observed even at low pH, in contrast to what was recorded for particles stabilized with unacetylated forms of ligands, **G4–G6** (Table 3). This confirms the assertion that hydrogen bonding plays a key role in the aggregation of glyco-thiol AuNPs. Once again, there was no major shift in the spr bands of **G9–G11** (Fig. 6) compared to citrate-capped AuNPs (519 nm), suggesting that the spherical morphology and integrity of the particles were maintained. This was confirmed by the TEM results showing spherical particles with an average size of *ca.* 14 nm (Fig. 7). In general, the surface charges of the **G6–G11**, as exhibited by the ζ-potential measurements, demonstrate stable negatively charged AuNPs. This is an indication that the AuNPs **G6–G11**, especially **G9**, **G10**, and **G11**, are stable and could be used as drug delivery carrier.

The nanoparticles **G6–G11** were subjected to a cellular environment with a high salt concentration (*ca.* 100 mM), to establish their stability under such conditions. This was done by adding up to a maximum of 1 mL (excess) of NaCl

Fig. 3 UV-vis spectra of AuNPs produced with different Au : **L3** ratios.

Table 3 Summary of pH and ζ-potential values and particle size of AuNPs

Ligands	**G6**		**G7**		**G8**		CGN[a]
Ligands pH	7.11	10.75	7.29	10.74	7.34	10.78	—
AuNPs pH	8.42	8.18	8.89	7.94	8.81	8.73	—
ξ-Potential/mV	−17.5	−23.7	−16.9	−23.4	—	−22.2	−37.5
Particle size/nm	14.3 ± 1	14.3 ± 1	14.4 ± 4	14.5 ± 1	—	14.6 ± 2	14.0
λ_{max}/m	535	522	523	522	—	521	519

[a] Citrate-capped gold nanoparticles.
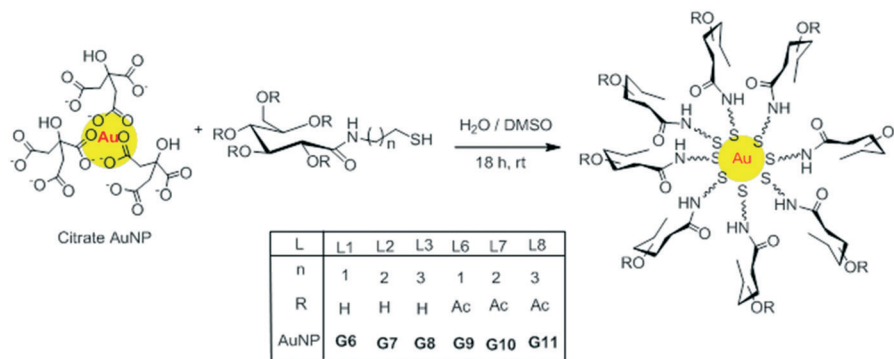
Scheme 2 Schematic representation for the replacement of the citrate ion by glyco thiol, acetylated glyco-thiols and thiolate compounds.

solution. Unlike the citrate-capped particles that agglomerate instantly (accompanied by a colour change to blue) upon addition of a few drops of NaCl, **G6–G11** were stable and did not change colour upon addition of excess 2 M NaCl. The particles remained stable for about five (5) days. This also validates the success of the ligand exchange process (citrate for glyco thiol ligands) on the surface of the AuNPs.

A standard electrophoresis experiment using 1.5% agarose gel with 1 M TBE buffer run at 80 V for 6 min was conducted to further prove that the ligand exchange process was successful and that the particles are stable (Fig. 8, see ESI† Fig. S9). Citrate-capped gold nanoparticles aggregate under the running conditions of gel electrophoresis (Fig. 8) due to the high ionic concentration of the running buffer, in agreement with the electrolyte test observation mentioned above (*vide supra*). The migration of the gold nanoparticles as shown in **G1–G11** in Fig. 8 indicates that the glyco thiolate stabilizes the particles fully and is negatively charged in agreement with the ζ-potential data.

The long chain glyco-thiol AuNPs **G3–G5** migrate toward the negative electrode, which confirms that they are positively charged as determined by ζ-potential measurements (Table 2). This is attributed to the increase in lipophilicity as a result of the increased alkyl chain. By plotting the pH titration measurements *versus* the ζ-potential measurements, in-

ferences about the dispersion stability of the nanoparticles were drawn.[31] The pH of AuNP solutions was varied by starting with a suspension of nanoparticles in double distilled water and then adding incremental amounts of either 2 M HCl or 2 M K_2CO_3 to adjust the pH between measurements. The pH of individual samples was varied in one direction (from neutral toward either low or high pH).

Fig. 9 illustrates the results of such titrations for concentrated dispersions of AuNPs (**G1** and **G6**) as representatives. It is seen that the iso-electric point of these two AuNPs is at 3 > pH > 13 (Fig. 9). However, the two AuNPs aggregate under these extreme pH conditions, a point where the red colour turned black and the ζ-potential values move closer to the isoelectric point. As the pH of **G1** and **G6** increased from 3 to 10, the ζ-potentials increase in magnitude from about −22 to *ca.* −55 mV (Fig. 9), indicating stable and well-dispersed particles; however the nanoparticle integrity is lost at 3 > pH > 10 leading to aggregation (Fig. 9). This is in agreement with the fact that nanoparticles with a ζ-potential above (±)30 mV are known to be stable in suspension as the surface charge prevents the aggregation of the particles.[32–34]

Generally, the maximum ζ-potentials of **G1** and **G6** were recorded at pH values in the basic range and fall off toward the acidic range of pH < 3. This is consistent with the results
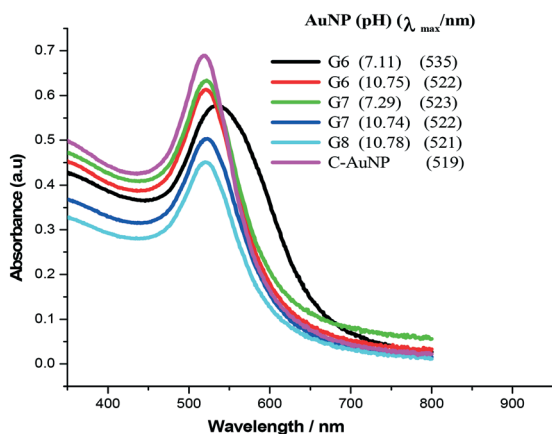
Fig. 5 UV-vis spectra of glyco-thiols (**G6–G8**) and citrate AuNPs.
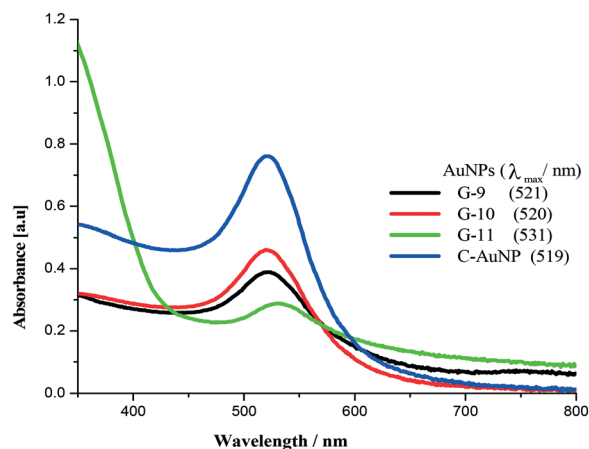
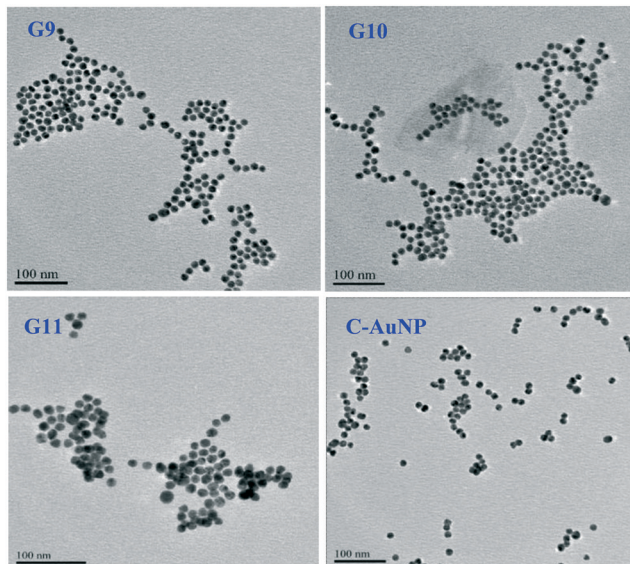**Fig. 6** UV-vis spectra of acetylated glyco thiol AuNPs (**G9–11**) and C-AuNPs.

Fig. 7 TEM images of ligand exchange AuNPs (**G9**–**G11**) and citrate AuNPs (C-AuNPs).

Fig. 9 Titration of pH against the ζ-potential of (A) acetylated and (B) non-acetylated glyco AuNPs.

reported for thiolate-modified gold particles where they showed −19.8, −55.7, −169.7 and −61.8 mV at pH of 3.5, 4.9, 6.7 and 9.4, respectively.[35] The aggregation of particles close to the isoelectric point and at extremely high pH was confirmed by the UV-vis spectra of AuNPs acquired at various pH values, which showed broad spectra and redshift of the absorption band at pH < 3 and extremely high pH > 13 (Fig. S4†). This result reaffirms the stable nature of our developed glyconanoparticles in a fairly large range of pH conditions.

In vitro anticancer screening of gold glyconanoparticles

Seven glyco-thiol gold nanoparticles prepared in this study, of sizes between 14 and 25 nm, were selected for biological
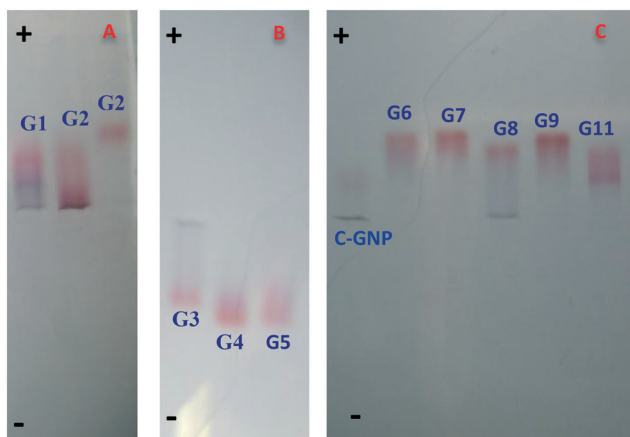

Fig. 8 Gel electrophoresis (1.5% agarose) in 1 M TBE buffer at 80 V for 60 min. (A) Direct method AuNPs of glyco-thiol (*n* = 1 and 2). (B) Direct method AuNPs of glyco-thiol (*n* 3, 4 and 5). (C) Ligand exchange AuNPs of non-acetylated glyco-thiol (*n* = 1–3), acetylated glyco-thiol (*n* = 1 and 3) and citrate AuNPs (C-GNP).
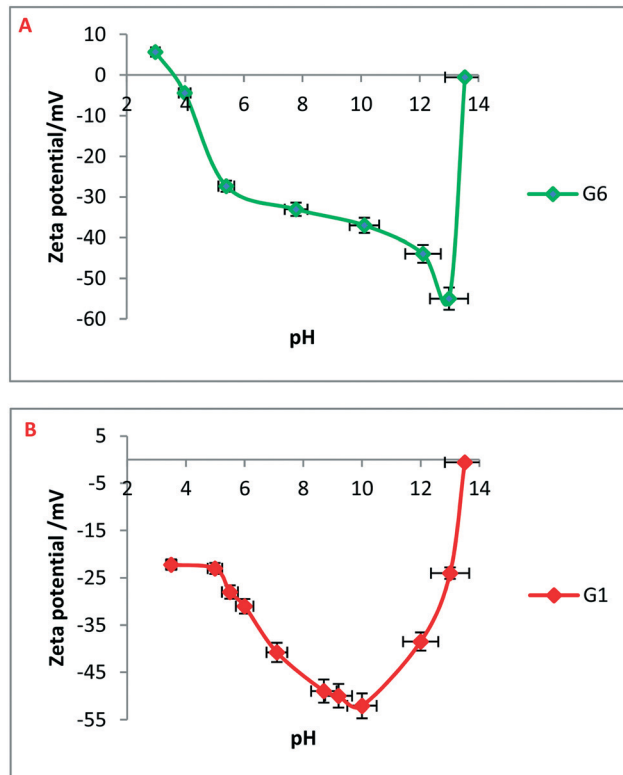
studies in order to investigate whether the new nanoparticles were toxic to normal cells or cytotoxic to cancerous cells. This was done to understand the biological activity profile of these monolayer nanoparticles because of the intention of using them as drug delivery vehicles. Human normal peripheral blood mononuclear cells (PBMCs) and the human lung adenocarcinoma epithelial cell line (A549) were used in this study. The A549 cancel cell line was chosen for the reason that, it is one of the poorly treated diseases.[36] The glyco moiety permits active targeting of the glyco micelles to cancer cells, specifically, those that express mannose receptors. A549 cells contain Man receptors all over the cell surface and however, these receptors may serve as target site to interact with glyco-thiol AuNPs.[37] This may perhaps be the reason why AuNP **G10** had quite good inhibition activity toward the lung cancer cell line as explained below (Table 4, Fig. S11†).

The activity profile shows that the glyconanoparticles were marginally active toward A549 cells with an IC_{50} ranging between 22.01 and >34.76 µg mL^{-1} (Table 4). The only exception was **G10**, which showed moderate activity toward A549 cells with an IC_{50} of 7.63 µg mL^{-1} (Table 4, Fig. 10 and S10†). The toxicity profile of AuNPs against the normal cells was similar to the activity profile of the nanoparticles against A549 cells except for **G10** that had an IC_{50} of >59.38 µg mL^{-1} suggesting its toxicity towards cancer cells. This indicates that while all other particles had indiscriminate effects on PBMCs and A549, **G10** had a different profile suggesting slight selectivity towards A549 cells compared with PBMCs.

Table 4 Summary of antitumor screening results showing glyconanoparticle IC$_{50}$ concentrations for different cell lines

AuNPs	Initial conc. of AuNP (μg mL^{-1})	Highest conc. of AuNP tested (μg mL^{-1})	Size (nm)	Cell line/IC$_{50}$ (μg mL^{-1} ± Std. dev)	
				PBMC	A549
G3	69.50	34.75	23.1	23.37 ± 2.40	22.01 ± 2.41
G4	69.35	34.65	16.0	33.13 ± 3.68	21.50 ± 6.08
G5	69.53	34.77	16.0	25.28 ± 5.01	13.97 ± 5.03
G9	118.76	59.38	14.0	38.41 ± 2.96	32.49 ± 2.46
G10	118.76	59.38	14.0	>59.38	7.63 ± 0.21
G11	118.76	59.38	14.0	37.15 ± 7.72	31.11 ± 1.51
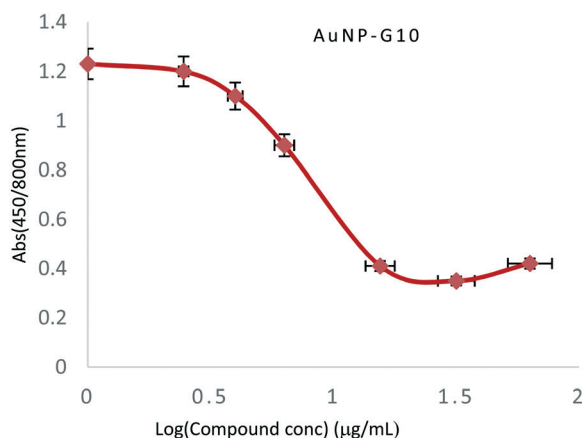
Fig. 10 Growth inhibition profile of **AuNP-G10** against the A549 cancer cell line.

This could be attributed to the fact that **G10** particles are acetylated glyconanoparticles and their hydrophobic nature allows them to cross the cancerous cell membrane more easily.[38] The present work agrees with the studies by Kudgus and co-workers who reported mannose DOX-conjugated AuNPs with an inhibitory concentration of 5.2 μM.[36] Yin and co-workers also reported glycopolymer nanoparticles of 50 μg mL^{-1}, 10 μg mL^{-1} and 250 μg mL^{-1} non-toxic doses against human lung carcinoma (A549) and other forms of cancer cell lines.[37]

Generally, there were no specific structural trends noted such as varying biological activity due to the chain length of the ligands. This, compared to our previous report of glyco thiolate particles synthesized *via* the Brust and Schiffrin NaBH$_4$ reduction method,[24] shows marginal improvement in activity and selectivity, probably due to the hydrophobic nature of some particles and relatively bigger sizes of the current particles even though they were tested on different cell lines. Suffice it to say that since the test compounds were marginally active, over a 4 day incubation period, the glyco thiol nanoparticles can be regarded as inactive and could be more useful as drug delivery vehicles.

Conclusions

The use of *n*-gluconamidoalkyl thiols and their acetylated forms to prepare and stabilize gold nanoparticles either di-

rectly or *via* ligand exchange procedures was studied extensively. The results presented show that these ligands can be used as reducing agents and stabilizing agents, too. Notably, the thiol ligands have to be activated, by preparing their potassium salts, to render them more reactive which invariably gives good monodispersed nanoparticles. Several techniques were employed to study the nanoparticles. UV-vis spectroscopy, ζ-potential measurement, and TEM techniques were employed to study the properties of these nanoparticles. Zeta potential measurements and pH studies clearly demonstrated that the glyco gold nanoparticles prepared in this study are quite stable, especially in alkaline medium. The direct synthesis method for making AuNPs, using short alkyl chain glyco thiols (n = 1 and 2) as reducing agents, gave negatively charged nanoparticles while the long alkyl chain (n = 3, 4 and 5) counterparts gave positively charged particles. This is rather unusual considering that the two sets of ligands are structurally similar and only differ in the chain length, and can only be attributed to the inductive effect of long alkyl chains. The TEM images showed that the spherical morphology of the AuNPs is dominant and is maintained, even in the gold nanoparticles prepared *via* substitution of the citrate with compounds **L1**–**L8**. TEM imaging and ζ-potential studies also showed that defined stable particles are formed as the chain length of glyco-thiol ligands is increased to $n \geq 3$. It can be concluded from these studies that the ligand concentration, pH, and chain length have an effect on the particle formation. *In vitro* anticancer screening of the glyco-thiol AuNPs prepared was generally inactive against PBMCs and A549 cells. This is a positive result as these glyconanoparticles could be employed as drug delivery systems. Thus, future work would include loading certain anticancer drugs and targeting peptides on the glyconanoparticles and investigate the efficacies of the resultant constructs against cancer cells.

Experimental

Materials and instrumentation

All materials and chemicals were used as received unless otherwise specified. Hydrogen tetrachloroaurate (HAuCl$_4$·3H$_2$O), potassium hydroxide and D-(+)-gluconic acid δ-lactone were purchased from Sigma Aldrich. 5-Aminopentane-1-thiol (APtT) and 6-amino hexane-1-thiol (AHT) were purchased from Ivy Fine Chemicals and used without further

purification. Gluconamidoalkyl thiols (**L1–L4**) (ESI†)[24] and citrate-capped 14 nm gold nanoparticles (**CG**)[7] were synthesized according to literature methods. All glassware was thoroughly cleaned with *aqua regia* and rinsed with double distilled water prior to use. All solutions were prepared using water purified with a Millipak (Millipore Q-POD) system 40 (0.22 pm) filtration system. The UV-vis absorption spectra (300–800 nm) of the AuNP samples were recorded on a Cary UV 100 spectrophotometer at room temperature. The size and morphology of the AuNPs were analyzed using a JEOL JEM 2100F transmission electron microscope fitted with a probe size of ~0.5 nm at 200 kV at MINTEK (South Africa). Zeta potential measurements were recorded using a Zetasizer Nano-ZS (MPT-2) (Malvern Instruments, Malvern, UK). The toxicity of the test gold glyconanoparticles was evaluated against peripheral blood mononuclear cells (PBMCs) including their potential cytotoxicity in the non-small cell lung carcinoma cell line A549 donated by the University of Pretoria to MINTEK. PBMCs were isolated from whole blood obtained from the MINTEK clinic (Private Bag X3015, Randburg, 2125, South Africa) using Ficoll-Paque gradient centrifugation and stimulated for 3 days with PHA-P, according to established literature procedures.[39]

All NMR (^{1}H and ^{13}C{^{1}H}) spectra were recorded in D_2O, d_6-DMSO and CDCl$_3$ and on a Bruker Ultrashield (400 MHz) spectrometer at room temperature. ^{1}H and ^{13}C chemical shifts were referenced to the residual signals of the protons or carbons of the NMR solvents and are quoted in ppm: D_2O at 4.65 ppm for ^{1}H and CDCl$_3$ at 7.24 and 77.50 ppm for ^{1}H and ^{13}C spectra, respectively. Infrared spectra were recorded on a Bruker Tensor 27 fitted with an ATP-IR probe and a Perkin Elmer FT-IR spectrometer BX. Raman spectra were recorded on a Perkin Elmer Raman Station 400 bench top Raman spectrometer. The excitation source was a near-infrared 785 nm laser (100 mW at the sample), with a spot size of 100 μm. A spectral range of 200–3200 cm^{-1} was employed. Elemental analysis was performed on a Vario Elementar III microcube CHNS analyzer at Rhodes University, South Africa. High resolution mass spectra were recorded in the ESI mode on a Waters API Quattro Micro spectrophotometer at the University of Stellenbosch, South Africa.

Synthesis of 5-gluconamidopentyl thiol (L4)

Compounds **L4** and **L5** were synthesized according to a previous method reported by Adokoh *et al.* 2015.[24] To a solution of D-(+)-gluconic acid δ-lactone (1.0 g, 5.61 mmol) in methanol (30 mL) was added 5-amino pentyl thiol (0.67 g, 5.63 mmol). The mixture was stirred overnight at room temperature and the white precipitate was filtered and washed with isopropanol and acetone to afford the white solid product of compound **L5**. Yield: 1.2 g (72%). ^{1}H NMR (D_2O, 400 MHz): δ_H 3.93 (dd, 1H, J = 4.8 Hz, H-2), 3.64 (d, 1H, J = 11.6, H-4), 3.57 (d, 1H, J = 7.2 Hz, H-3), 3.49 (s, 2H, H-6), 3.44 (q, 2H, J = 6.4 H-6), 3.08 (t, 1H, J = 6.8 Hz, H-5), 2.83 (t, 2H, J = 7.6 –NCH$_2$–), 1.51 (m, 2H, –CH$_2$SH), 1.40 (m, 3H, –CH$_3$–), 1.24

(m, 3H, –CH$_3$–) (Fig. S5a†); ^{13}C{^{1}H} NMR (D_2O, 100 MHz): δ_C 174.4 (C-1), 73.4 (C-2), 72.1 (C-3), 71.5 (C-4), 71.1 (C-5), 70.4 (C-6), 37.8 (–NCH$_2$–), 36.6 (–CH$_2$–), 36.6 (–CH$_2$–), 36.5 (–CH$_2$–), 17.4 (–CH$_2$SH–); (Fig. S6†) FT-IR (neat, cm^{-1}): 3298 ν(O–H), 2946 ν(C–H), 1733 ν(C=O), 1655 ν(N–H), 1439 ν(CH$_2$), 1217 ν(C–N), 1129 ν(C–S), 1038 ν(C–O) (Fig. S5b†). Anal. calcd. for C$_{11}$H$_{23}$O$_6$NS: C, 44.39; H 7.80; N, 4.35; S, 10.78; found: C, 42.43; H, 8.13; N, 4.80; S, 9.89. HRMS (ESI): *m/z* (M$^+$) calcd. 297.1246; found: 297.1530.

Synthesis of 6-gluconamidohexyl thiol (L5)

A similar procedure used for **L4** synthesis was employed for **L5** synthesis with the following reagents: 6-aminohexyl thiol (0.75 g, 5.63 mmol) and D-(+)-gluconic acid δ-lactone (1.0 g, 5.61 mmol). Yield: 1.0 g (57%). ^{1}H NMR (D_2O, 400 MHz): δ_H 4.09 (s, 1H, H-2), 3.98 (s, 1H, H-3), 3.65 (t, 1H, J = 5.2 Hz, H-4), 3.52 (t, 1H, J = 5.2, Hz H-5), 3.46 (q, 2H, J = 6.4 Hz, H-6), 3.15 (t, J = 5.6 Hz, 2H, –NCH$_2$), 2.83 (t, 2H, J = 7.6 Hz, H-8), 1.62 (t, 2H, J = 7.2 Hz, H-12), 1.49 (m, 6H, H9–11). ^{13}C{^{1}H} NMR (D_2O, 100 MHz): δ_C 174.3 (C-1), 73.4 (C-2), 72.2 (C-3), 71.1 (C-4), 70.3 (C-5), 62.6 (C-6), 37.6 (–NCH$_2$–), 35.1 (–CH$_2$–), 38.0 (–CH$_2$–), 28.0 (–CH$_2$–), 17.4 (–CH$_2$SH–); FT-IR (neat, cm^{-1}): 3281 ν(O–H), 2939 ν(C–H), 1735 ν(C=O), 1590 ν(N–H), 1377 ν(CH$_2$), 1219 ν(C–N), 1022 ν(C–O). Anal. calcd. for C$_{12}$H$_{25}$O$_6$NS: C, 46.28; H 8.09; N, 4.50; S, 10.30; found: C, 45.95; H, 8.12; N, 4.01; S, 9.79. HRMS (ESI): *m/z* (M$^+$) calcd. 311.1403; found: 311.1444 (Fig. S8†).

Glyco-thiolate gold nanoparticle synthesis

Direct method of glyco thiolate gold nanoparticle synthesis (G1–G5)

In a typical experiment, 1 mL of 1% HAuCl$_4$·3H$_2$O (0.01 g, 2.54 mmol) was added to pre-heated double distilled water (150 mL) in a round bottom flask. The light yellow solution was brought to boiling while vigorous stirring before addition of various concentrations of aqueous solution of potassium salt (1 equiv.) of **L1** (see Table 2 for details). There was an immediate colour change to red-brown. The reaction mixture was allowed to stir for another 3 min and the resultant AuNPs, **G1**, were cooled and filtered. A similar procedure was repeated but with potassium salts of ligands **L2–L5** (see Tables 1 and 2 for details) to give **G2–G5** nanoparticles, respectively. In addition, different gold : ligand molar ratios were used to prepare sets of **G4–G5** nanoparticles, using the above procedure, for ligand concentration studies. Yield = 69.35–69.50 μg mL^{-1}.

Synthesis of glyco thiolate gold nanoparticles *via* the ligand exchange method (G6–G8)

Aqueous solutions of gluconamidoalkyl thiols (**L1–L3**) (10 μg mL^{-1}, 12 μL) were added to three different portions of 12 mL of red gold citrate-capped AuNPs (**CG**) (14 nm) at room temperature and left to gently stir overnight. No major colour

variation was observed. The reaction mixture was then centrifuged and washed with double distilled water three times in succession. The final product was re-suspended in distilled water. Yield = 118.76 μg mL^{-1}.

Synthesis of acetylated glyco thiol-gold nanoparticles *via* the ligand exchange method (G7–G9)

In the second part of the experiment, **G7–G9** were prepared as **G6–G8** but with 50% DMSO solutions of **L4–L6** (10 μg mL^{-1}, 12 μL). The red colloidal suspension turned deep red within 3 h and dark red over 8 h. Yield = 118.76 μg mL^{-1}.

pH measurements

The pH measurements of the AuNPs were done using a Basic-20 pH meter, which was calibrated using buffer solutions of pH 4.0, 7.0 and 9.0. The pH of the analyte was adjusted using either K_2CO_3 or NaOH. The electrode was rinsed with double distilled water after every successive measurement.

Cytotoxicity screening of gold nanoparticles (test compounds) in PBMCs and A549 cells

The cells were treated with the test compounds and their survival measured using the Cell Titer aqueous non-radioactive assay (Promega Corporation, Madison, Wisconsin, USA).[40,41] PBMCs or A549 cells were seeded into 96-well microtiter plates at a low passage number, at a concentration of 2×10^5 cells per mL with each well having a total volume of 100 μL complete RPMI 1640 medium. The medium contained 10% fetal bovine serum (FBS, Highveld Biological, and R.S.A.) and streptomycin. The cells were incubated for 24 h at 37 °C and 5% CO_2 before the test compounds were added in two-fold serial dilutions with concentrations ranging from 35 to 110 μg mL^{-1} (Table 4) considering the gravitational settling and expressing the dose in terms of mass per unit surface area of the culture dish (μg cm^{-2}).[42] The cells were incubated for another 96 h, before 10 μL per well of the Cell Titer solution was added to the cells, and gently mixed before incubating the plates under previously described conditions (*vide supra*). The plates were read after every 2 h at an absorbance wavelength of 490 nm on a multiplate reader (xMarkTM, Bio-Rad). The IC$_{50}$ values were determined as the concentrations of the test substances required to reduce cell viability by 50% using OriginPro® version 8.0 software (OriginLab Corporation, Northampton, MA 01060 USA).

Conflicts of interest

There are no conflicts to declare.

Acknowledgements

References

1 E. Dulkeith, M. Ringler, T. A. Klar, J. Feldman, A. M. Javier and W. J. Parak, *Nano Lett.*, 2005, **5**, 585–589.

2 G. F. Paciotti, L. Myer, D. Weinreich, D. Goia, N. Pavel, R. E. McLaughlin and L. Tamarkin, *Drug Delivery*, 2004, **11**, 169–183.

3 Y. Kim, R. C. Johnson and J. T. Hupp, *Nano Lett.*, 2001, **1**, 165–167.

4 J. Luo, V. W. Jones, M. M. Maye, L. N. Han, N. Kariuki and C. J. Zhong, *J. Am. Chem. Soc.*, 2002, **124**, 13988–13989.

5 J. F. Hicks, F. P. Zamborini, A. J. Osisek and R. W. Murray, *J. Am. Chem. Soc.*, 2001, **123**, 7048–7053.

6 A. J. Mieszawska, W. J. M. Mulder, Z. A. Fayad and D. P. Cormode, *Mol. Pharmacol.*, 2013, **10**, 831–847.

7 J. Turkevich, P. C. Stevenson and J. Hillier, *Discuss. Faraday Soc.*, 1951, **11**, 55–75.

8 G. Frens, *Colloid Polym. Sci.*, 1972, **250**, 736–741.

9 G. Frens, *Nat. Phys. Sci.*, 1973, **241**, 20–22.

10 K. R. Brown and M. J. Natan, *Langmuir*, 1998, **14**, 726–728.

11 N. R. Jana, L. Gearheart and C. Murphy, *J. Adv. Mater.*, 2001, **13**, 1389–1393.

12 N. R. Jana, L. Gearheart and C. J. Murphy, *J. Phys. Chem. B*, 2001, **105**, 4065–4067.

13 K. Subrata, P. Sudipa, P. Snigdhamayee, B. Soumen, K. Sujit, P. Anjali and P. Tarasankar, *Nanotechnology*, 2007, **18**, 075712.

14 K. E. Sapsford, W. R. Algar, L. Berti, K. B. Gemmill, B. J. Casey, E. Oh, M. H. Stewart and I. L. Medintz, *Chem. Rev.*, 2013, **113**, 1904–2074.

15 M. J. De la Fuente, G. A. Barrientos, C. T. Rojas, J. Rojo, J. Canada, A. Fernandez and S. Penades, *Angew. Chem.*, 2001, **113**, 2318–2321.

16 G. A. Barrientos, M. J. De la Fuente, C. T. Rojas, A. Fernandez and S. Penades, *Chem. – Eur. J.*, 2003, **9**, 1909–1921.

17 M. J. De la Fuente, D. Alcantara and S. Penades, *IEEE Trans. Nanobioscience*, 2007, **6**, 275–281.

18 F. Compostella, O. Pitirollo, A. Silvestri and L. Polito, *Beilstein J. Org. Chem.*, 2017, **13**, 1008–1021.

19 N. M. Adams, S. R. Jackson, F. R. Haselton and D. W. Wright, *Langmuir*, 2012, **28**, 1068–1082.

20 J. Wu, M. H. Nantz and M. A. Zern, *Front. Biosci.*, 2002, **7**, d717–d725.

21 M. Hashida, M. Nishikawa, F. Yamashita and Y. Takakura, *Adv. Drug Delivery Rev.*, 2001, **19**(52), 187–196.

22 J. M. De la Fuente and S. Penadés, *Biochim. Biophys. Acta*, 2006, **1760**, 636–651.

23 R. Ojeda, J. L. de Paz and A. G. Barrientos, *et al.*, *Carbohydr. Res.*, 2007, **342**, 448–459.

24 C. K. Adokoh, C. Obuah, O. Zinyemba, H. H. Kinfe and J. Darkwa, *New J. Chem.*, 2015, **39**, 5249–5258.

25 S.-Y. Lin, Y.-T. Tsai, C.-C. Chen, C.-M. Lin and C.-H. Chen, *J. Phys. Chem. B*, 2004, **108**, 2134–2139.

26 C. N. R. Rao, A. K. Sood, K. S. Subrahmanyam and A. Govindaraj, *Angew. Chem., Int. Ed.*, 2009, **48**, 7752–7777.

27 S. Luis, *Educ. Quim.*, 2017, **28**, 232–237.

28 A. Majzik, R. Patakfalvi, V. Hornok and I. Dékány, *Gold Bull.*, 2009, **42**, 113–123.

29 A. Mocanua, I. Cernicab, G. Tomoaiac, L.-D. Bobosa, O. Horovitz and M. Tomoaia-Cotisel, *Colloids Surf., A*, 2009, **338**, 93–101.

30 S. Aryal, B. K. C. Remant, N. Dharmaraj, N. Bhattarai, C. H. Kim and H. Y. Kim, *Spectrochim. Acta, Part A*, 2006, **63**, 160–163.

31 S. Fazio, J. Guzman, M. T. Colomer, A. Salomoni and R. Moreno, *J. Eur. Ceram. Soc.*, 2008, **28**, 2171–2176.

32 V. Mohanraj and Y. Chen, *J. Pharmacol. Res.*, 2006, **5**, 561–573.

33 N. Düzgüneș, *Nanomedicine: Infectious Diseases, Immunotherapy, Diagnostics, Antifibrotics, Toxicology and Gene Medicine*, 1st edn, 2012, vol. 509, pp. 133–134.

34 A. Tiwari and A. Tiwari, *Bioengineered Nanomaterials*, Taylor and Francis group, CRC press, New York, 2014, p. 303.

35 K. Kimura, S. Takashima and H. Ohshima, *J. Phys. Chem. B*, 2002, **106**, 7260–7266.

36 R. A. Kudgus, R. Bhattacharya and P. Mukherjee, *Anti-Cancer Agents Med. Chem.*, 2011, **11**, 965–973.

37 L. Yin, Y. Chen, Q. Yin, Z. Zhang, Q. Yin, N. Zheng and J. Cheng, *Macromol. Rapid Commun.*, 2015, **36**, 483–489.

38 F. Caruso, M. Rossi, J. Tanski, C. Pettinari and F. Marchetti, *J. Med. Chem.*, 2003, **46**, 1737.

39 D. Devine, *et al.* Antiviral Methods and Protocols, in *Methods in Molecular Medicine*, ed. D. Kinchington and R. F. Schinazi, Humana Press Inc., Totowa, NJ, U.S.A., 2000, vol. 24, p. 196.

40 J. A. Barltrop, T. C. Owen, A. H. Cory and J. G. Cory, *Bioorg. Med. Chem. Lett.*, 1991, **1**, 611–614.

41 A. H. Cory, T. C. Owen, J. A. Barltrop and J. G. Cory, *Cancer Commun.*, 1991, **3**, 207–212.

42 J. G. Teeguarden, P. M. Hinderliter, G. Orr, B. D. Thrall and J. G. Pounds, *Toxicol. Sci.*, 2007, **95**, 300–312.